Mitigating Pathogenesis for Target Discovery and Disease Subtyping

Eric V. Strobl, Thomas A. Lasko, Eric R. Gamazon

***Abstract*— Treatments ideally mitigate pathogenesis, or the detrimental effects of the root causes of disease. However, existing definitions of treatment effect fail to account for pathogenic mechanism. We therefore introduce the *Treated Root causal Effects* (TRE) metric which measures the ability of a treatment to modify root causal effects. We leverage TREs to automatically identify treatment targets and cluster patients who respond similarly to treatment. The proposed algorithm learns a partially linear causal model to extract the root causal effects of each variable and then estimates TREs for target discovery and downstream subtyping. We maintain interpretability even without assuming an invertible structural equation model. Experiments across a range of datasets corroborate the generality of the proposed approach.**

***Index Terms*— root causes, target discovery, pathogenesis, causal inference, precision medicine**

I. Introduction

Target discovery refers to the process of identifying disease-modifying targets for the development of novel treatments. Candidate targets should causally affect patient symptoms. We seek to discover treatment targets from data with minimal prior knowledge, time and expense.

Properly identifying treatment targets requires a careful definition of treatment effect. Most investigators quantify treatment effect using counterfactuals or the do-operator found in the causal inference literature [1], [2]. Unfortunately, these quantities ignore the effect of treatment on pathogenesis. Consider for example the following causal graph in a patient with appendicitis:

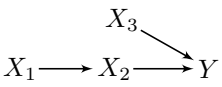

where fecal impaction X_1 causes bacterial inflammation of the appendix X_2 which in turn causes lower abdominal pain Y [3]. We can treat the patient with opioids or other pain medications X_3 that directly act on Y. However, these medications ignore the pathogenesis of impaction and inflammation leading to the lower abdominal pain. We need definitive treatments that remove the inflammation (e.g., antibiotics) or both the impaction and inflammation (appendectomy). We thus seek a new definition of treatment effect that accounts for the ability of a treatment to modulate pathogenic mechanism.

A pathogenically informed formulation of treatment effect may also assist with diagnosis. Modern clinical diagnoses of complex diseases, such as schizophrenia, fail to map onto the few biological targets needed for potent treatment development [4]–[6]. Investigators have therefore proposed to discover *theratypes*, or disease categories that delineate patients with distinct responses to potentially undiscovered treatments [7]. For example, physicians once categorized anemia as a single disease. Further research revealed the presence of multiple subtypes, such as those responsive to iron and vitamin B12 supplementation [8], [9]. We now categorize iron and vitamin B12 deficiency-induced anemia as two distinct theratypes. This example suggests that we can identify theratypes directly by their differential treatment effects – provided that the treatment effects properly account for pathogenesis.

We make the following contributions in this paper:

(1) We summarize the causal effects associated with pathogenesis using the *root causal effects*, or the causal effects of the root causes of disease.
(2) We measure treatment effect using the *Treated Root causal Effects* (TRE) metric that quantifies the ability of a treatment to change the root causal effects.
(3) We introduce an algorithm that estimates the root causal effects and TREs from observational data under a partially linear model.
(4) We employ hierarchical clustering of the estimated TREs to identify theratypes such that grouped patients have pathogenic mechanisms responding similarly to targeted treatments.

Experiments highlight the generality of the approach by demonstrating markedly improved performance across a range of datasets.

II. Background

We can formally represent a causal process over a set of $p+1$ *endogenous* variables $\boldsymbol{X}$ using a structural equation model (SEM) linking the variables with deterministic functions and error terms:

$$X_i = f_i(\text{Pa}(X_i), E_i), \qquad \forall X_i \in \boldsymbol{X}, \tag{1}$$

where $\boldsymbol{E}$ is a set of mutually independent and *exogenous* error terms. The set $\text{Pa}(X_i) \subseteq \boldsymbol{X} \setminus X_i$ corresponds to the *parents* of X_i. We call X_i a *child* of X_j if $X_j \in \text{Pa}(X_i)$. If $\text{Pa}(X_i) = \emptyset$, then X_i is a *root vertex*. We assume $X_i = E_i$ if X_i is a root vertex without loss of generality. We can recover the error

term values uniquely from the endogenous variable values in an *invertible* SEM [10].

We associate a directed graph $\mathbb{G}$ to an SEM by drawing a directed edge from each $X_j \in \text{Pa}(X_i)$ to X_i for every $X_i \in \boldsymbol{X}$. A *directed path* from X_i to X_j corresponds to a sequence of adjacent directed edges from X_i to X_j. X_i is an *ancestor* or *cause* of X_j, and X_j is a *descendant* of X_i, if there exists a directed path from X_i to X_j (or $X_i = X_j$). We collect all ancestors and descendants of X_i into the sets $\text{Anc}(X_i)$ and $\text{Dec}(X_i)$, respectively. A *cycle* exists if there is a directed path from X_i to X_j, and the directed edge $X_j \to X_i$. A directed graph is called a *directed acyclic graph* (DAG) if it contains no cycles. We assume that $\mathbb{G}$ is a DAG throughout. If we have $X_i \to X_j \leftarrow X_k$, then we call X_j a *collider*. Two variables X_i and X_j are *d-connected* given $\boldsymbol{W} \subseteq \boldsymbol{X} \setminus \{X_i, X_j\}$ in $\mathbb{G}$ if there exists a path between X_i and X_j such that every collider on the path is an ancestor of $\boldsymbol{W}$ and no non-collider on the path is in $\boldsymbol{W}$. The two vertices are *d-separated* if they are not d-connected. If an SEM associated with a DAG obeys Equation (1), then the joint distribution over $\boldsymbol{X}$ satisfies the *global Markov property* such that d-separation between X_i and X_j given $\boldsymbol{W}$ implies conditional independence between X_i and X_j given $\boldsymbol{W}$ [11].

The *do-operator* $\text{do}(\boldsymbol{A} = \boldsymbol{a})$ represents a *treatment* (also known as an *intervention*), where we manually set the values of $\boldsymbol{A} \subseteq \boldsymbol{X}$ to $\boldsymbol{a}$ by replacing f_i for each $X_i \in \boldsymbol{A}$ in Equation (1) with $X_i = x_i$. We write $\text{do}(\boldsymbol{a})$ for shorthand and associate the treatment with the graph $\mathbb{G}_{\text{do}(\boldsymbol{a})}$ obtained by removing the directed edges into each member of $\boldsymbol{A}$ from $\mathbb{G}$. We have $E_i = X_i = x_i$ for any $X_i \in \boldsymbol{A}$ after the do-operation because $\boldsymbol{A}$ only contains root vertices in $\mathbb{G}_{\text{do}(\boldsymbol{a})}$. The notation $\text{do}(\boldsymbol{A}, \boldsymbol{b})$ similarly means that we remove the directed edges into each member of $\boldsymbol{A} \cup \boldsymbol{B}$ from $\mathbb{G}$ to create $\mathbb{G}_{\text{do}(\boldsymbol{A},\boldsymbol{b})}$. We replace f_i for each $X_i \in \boldsymbol{A}$ in Equation (1) with $X_i = X_i$, and replace f_i for each $X_i \in \boldsymbol{B}$ with $X_i = x_i$.

A linear SEM obeys the following form:

$$X_i = \boldsymbol{X}\beta_{\cdot i} + E_i, \qquad \forall X_i \in \boldsymbol{X}, \tag{2}$$

where $\beta_{ji} \neq 0$ if and only if $X_j \in \text{Pa}(X_i)$. We assume $\mathbb{E}(\boldsymbol{X}) = 0$. If the error terms follow continuous non-Gaussian distributions, then we more specifically refer to Equation (2) as the Linear Non-Gaussian Acyclic Model (LiNGAM); LiNGAM is invertible [12]. We can rewrite the above equation in matrix form:

$$\boldsymbol{X} = \boldsymbol{X}\beta + \boldsymbol{E} = \boldsymbol{E}(I - \beta)^{-1} = \boldsymbol{E}\Theta,$$

where Θ denotes the matrix of *total effects* of $\boldsymbol{E}$ on $\boldsymbol{X}$. Let θ refer to the column vector in Θ associated with a target $Y = X_{p+1} \in \boldsymbol{X}$. We can *augment* $\mathbb{G}$ by including directed edges from each E_i to X_i except when $X_i = E_i$ is already a root vertex. We display the augmented graph for the appendicitis example below:

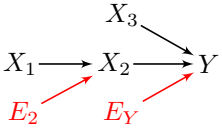

The *root causes* of Y correspond to root vertices that are ancestors of Y in the augmented graph [13]. If E_i is a root cause of Y, then X_i is the projection of the error term onto $\boldsymbol{X}$, and $E_i\theta_i$ is the *root causal effect* of X_i on Y [14], [15]. We have $X_3 = 0$ (no pain medications) in the appendicitis example even though $\theta_3 = \beta_{3Y} \neq 0$, so that the root causal effect of X_3 on Y is zero before treatment. Note that we define root causes and their effects relative to the observed variables $\boldsymbol{X}$; if $X_i = E_i$ is a root cause of Y for $\boldsymbol{X}$, but unobserved X_{p+2} has a non-zero total effect on Y with $X_{p+2} \to X_i$, then X_{p+2} is a root cause of Y for $\boldsymbol{X} \cup X_{p+2}$ but not for $\boldsymbol{X}$.

III. Related Work

We will identify treatment targets by quantifying their ability to modulate root causal effects on a phenotypic response Y. However, most investigators currently identify treatment targets with high throughput screening, where they test the causal effects of a large number of molecules on a disease phenotype or target assay [16]. The process incurs substantial cost and time partly because most high throughput screens ignore the pathogenic mechanisms underlying the disease.

Investigators have thus also designed algorithms that identify treatment targets by incorporating knowledge of biological networks [17], [18]. Many methods represent the network using an undirected graph, where edges denote statistical associations or binding affinities. Scientists then utilize measures of proximity or centrality to predict treatment effect [19]. Unfortunately, these quantities predict treatment effect inaccurately because the undirected edges fail to capture biologically plausible causal relations.

A third set of methods utilize directed graphs, where directed edges encode causal relationships. These methods estimate the causal effect of X_i on Y via $\mathbb{P}(Y|\text{do}(x_i))$, or similarly $\mathbb{E}(Y|\text{do}(x_i))$, from observational data by conditioning and then marginalizing over an appropriate subset of the variables [20]–[22]. The conditional distribution quantifies the causal effect of X_i on Y, but it does not consider the *root* causal effect of X_i on Y or the response of the root causal effects to treatment. Accounting for interactions using do- or asymmetric Shapley values fails to rectify the issues [23], [24]. We therefore cannot use these algorithms to discover treatments that mitigate pathogenesis.

We can however summarize the causal effects involved in pathogenesis using the root causal effects, or the total effects of all root causes on a phenotypic response Y. Investigators defined the root causal effect of a variable as the predictivity of its error term in a structural equation model [13], [14], [25]. They then proposed to use the Shapley values of [26] – equivalent to the root causal effects in the linear case – in order to identify the root causes of a target vertex. Operationalizing this idea requires invertible SEMs, where we can pinpoint the error term values from the endogenous variables alone. Unfortunately, nature may not obey the bijective relationships needed to recover the error terms exactly. The root causal effects also summarize pathogenic effects but do not quantify their response to treatment.

In this paper, we introduce an algorithm that measures the sample-specific effect of treatment on pathogenesis without

relying on the presence of bijective causal relationships. We assume that we can recover a DAG associated with a potentially non-invertible SEM. We then utilize the graph and the endogenous variables alone to recover the root causal effects. Subsequently, we introduce targeted interventions into the DAG and quantify how each intervention changes the total effects from root causes to phenotype Y. Clustering of the resultant changes yields groups of patients whose potentially differing pathogeneses respond similarly to treatment.

IV. Setup

A. Partially Linear Model

We consider an SEM obeying Equation (1) but enforce a linear SEM in the subset $\text{Anc}(Y) \subseteq \boldsymbol{X}$ so that:

$$X_i = \boldsymbol{X}\beta_{\cdot i} + E_i, \qquad \forall X_i \in \text{Anc}(Y).$$

The SEM therefore obeys a partially linear model. The error terms may be Gaussian or discrete, so we do not assume LiNGAM even among $\text{Anc}(Y)$. The following result holds:

Theorem 1. *The root causal effect of X_i on Y corresponds to the total effect of E_i on Y, or $E_i\theta_i$, under the partially linear model.*

We delegate proofs to the Appendix, unless explicated in the main text.

B. Motivating Example

Pathogenesis refers to the development of disease starting from its root causes and ending at its phenotype. We can therefore summarize the pathogenic causal effects using the root causal effects on a phenotypic label Y [13]–[15], [25]. Root causal effects may however differ from treatment response. Consider for example the following augmented causal graph:

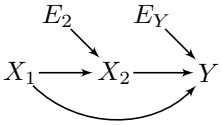

with binary error terms $E_1 = X_1$ and E_2 whose values are enumerated in Table I (a). We assume that $\beta = 1$, so that the root causal effects correspond to Table I (b).

We next introduce treatments that target specific nodes in $\boldsymbol{X}$. Let $\theta_{i|j}$ denote the total effect of E_i on Y after performing $\text{do}(X_j = x_j)$. If we set $\text{do}(X_1 = -1)$, then the root causal effects correspond to the values listed on the left side of Table I (c). Similarly, if we set $\text{do}(X_2 = 0)$, then we obtain the right side. We list the treatment responses in Table I (d) corresponding to the overall change in root causal effects between Tables I (b) and I (c). We highlight three observations:

(1) Different root causal effects may respond similarly to treatment. The red boxes highlight two cases where the root causal effects of X_2 are different in Table I (b) but have no treatment response after $\text{do}(X_2 = 0)$ in Table I (d).
(2) Patients may have partially matching root causal effects but entirely different treatment responses. The blue boxes in Table I (b) highlight two cases with the same root causal effects $E_2\theta_2$. However, the treatment responses for the two cases do not match after either $\text{do}(X_1 = -1)$ or $\text{do}(X_2 = 0)$ in Table I (d).
(3) Patients can have non-zero root causal effects but fail to respond to treatment. For example, the second blue box in Table I (b) has non-zero root causal effects but zero treatment responses in Table I (d).

Root causal effects without treatment thus provide insufficient information to predict treatment response. We instead want to quantify the change in root causal effects from before to after treatment.

V. Strategy

A. Overview

We now introduce a generalized strategy for identifying the change in root causal effects. We focus on the partially linear model for interpretability. In particular, we consider the p error terms that represent potential root causes:

$$E_1, \quad E_2, \quad \cdots \quad E_p.$$

We then weigh each error term by its total effect on a target variable Y:

$$E_1\theta_1, \quad E_2\theta_2, \quad \cdots \quad E_p\theta_p,$$

where $\theta_i = 0$ if $X_i \notin \text{Anc}(Y)$. We therefore predict the downstream target using the upstream error terms. We will show how to directly recover the above root causal effects even in non-invertible SEMs in the next section.

We next measure the change in the root causal effect of $X_i \in \boldsymbol{X} \setminus Y$ on Y after performing $\text{do}(X_j = x_j)$ with $X_j \in \boldsymbol{X} \setminus Y$:

$$\Delta_{i|j} = E_{i|j}\theta_{i|j} - E_i\theta_i,$$

where $E_{i|j} = E_i$ if $X_i \neq X_j$ and $E_{i|j} = x_j$ otherwise. The quantity $\sum_{i=1}^{p} \Delta_{i|j}$ corresponds to the *Treated Root causal Effects* (TRE) quantifying the change in the root causal effects

(a)

E_1	E_2
1	1
1	-1
-1	1
-1	-1

(b)

$E_1\theta_1$	$E_2\theta_2$
2	1
2	-1
-2	1
-2	-1

(c)

$\text{do}(X_1 = -1)$		$\text{do}(X_2 = 0)$	
$X_1\theta_{1\|1}$	$E_2\theta_{2\|1}$	$E_1\theta_{1\|2}$	$X_2\theta_{2\|2}$
-2	1	1	0
-2	-1	1	0
-2	1	-1	0
-2	-1	-1	0

(d)

$\text{do}(X_1 = -1)$	$\text{do}(X_2 = 0)$
$(X_1\theta_{1\|1} - E_1\theta_1)$ $+E_2(\theta_{2\|1} - \theta_2)$	$E_1(\theta_{1\|2} - \theta_1)$ $+(X_2\theta_{2\|2} - E_2\theta_2)$
-4	-2
-4	0
0	0
0	2

TABLE I: Example of the differences between root causal effects and treatment response.

on Y after intervening on X_j. This process leads to the feature space Π:

$$\sum_{i=1}^{p} \Delta_{i|1}, \quad \sum_{i=1}^{p} \Delta_{i|2}, \quad \cdots \quad \sum_{i=1}^{p} \Delta_{i|p} \tag{3}$$

summarizing the TRE for each $X_j \in \boldsymbol{X} \setminus Y$. If larger values of Y correspond to worse symptoms, then we prefer targets associated with negative TREs because they reduce symptoms. We also propose to perform clustering on Π in order to identify theratypes (details in Section V-E).

B. Endogenous Root Causal Effects

Recovering the root causal effect $E_i\theta_i$ for each sample requires access to the error term values. We cannot recover the error term values exactly in non-invertible SEMs. We remedy this situation with an alternative approach.

We can write the following using Equation (1):

Lemma 1. *We have* $\mathbb{P}(Y|E_i, \text{Pa}(X_i)) = \mathbb{P}(Y|X_i, \text{Pa}(X_i))$.

We thus no longer require knowledge of the value of E_i but only the values of the endogenous variables X_i and $\text{Pa}(X_i)$. Particularizing the above result to conditional expectations yields:

Corollary 1. *We have* $\mathbb{E}(Y|E_i, \text{Pa}(X_i)) = \mathbb{E}(Y|X_i, \text{Pa}(X_i))$.

The above corollary allows us to state:

$$\begin{aligned} \phi_i &\triangleq \mathbb{E}(Y|X_i, \text{Pa}(X_i)) - \mathbb{E}(Y|\text{Pa}(X_i)) \\ &= \mathbb{E}(Y|E_i, \text{Pa}(X_i)) - \mathbb{E}(Y|\text{Pa}(X_i)). \end{aligned} \tag{4}$$

Let $\boldsymbol{p}$ index $\text{Pa}(X_i)$ in $\boldsymbol{X}$. The conditional expectations in the last line correspond to the following under the partially linear model:

$$\begin{aligned} \phi_i &= \left(E_i\theta_i + \text{Pa}(X_i)\theta_{\boldsymbol{p}|\boldsymbol{p}}\right) - \text{Pa}(X_i)\theta_{\boldsymbol{p}|\boldsymbol{p}} \\ &= E_i\theta_i, \end{aligned} \tag{5}$$

where $\theta_{\boldsymbol{p}|\boldsymbol{p}}$ corresponds to the total effect of $\text{Pa}(X_i)$ on Y in $\mathbb{G}_{\text{do}(\text{Pa}(X_i))}$. We can therefore compute the root causal effect of X_i on Y using the difference $\mathbb{E}(Y|X_i, \text{Pa}(X_i)) - \mathbb{E}(Y|\text{Pa}(X_i))$ relying on endogenous variables alone. We have proved the following main result:

Theorem 2. *The root causal effect of X_i on Y corresponds to $\phi_i = \mathbb{E}(Y|X_i, \text{Pa}(X_i)) - \mathbb{E}(Y|\text{Pa}(X_i)) = E_i\theta_i$ under the partially linear model.*

C. Treated Root Causal Effects

We now consider the changes to the root causal effects introduced by targeted treatment. Suppose that we set the value of a variable X_j to x_j. We quantify the root causal effect of any variable X_i under $\text{do}(X_j = x_j)$ as follows:

$$\phi_{i|j} \triangleq E_{i|j}\theta_{i|j}$$

analogous to $\phi_i = E_i\theta_i$. The change in the root causal effect after treatment then corresponds to:

$$\Delta_{i|j} = \phi_{i|j} - \phi_i.$$

Repeating the above process for every $X_i \in \boldsymbol{X} \setminus Y$ allows us to compute $\sum_{i=1}^{p} \Delta_{i|j}$ for each $X_j \in \boldsymbol{X} \setminus Y$ and therefore the TREs in Expression (3).

We showed how to compute ϕ_i of each $\Delta_{i|j}$ in the previous section. We can compute $\phi_{i|j}$ given the coefficient matrix β over $\text{Anc}(Y)$ as follows. Let $\theta_{\boldsymbol{p}|\boldsymbol{p}j}$ correspond to the total effect of $\text{Pa}(X_i)$ on Y in $\mathbb{G}_{\text{do}(\text{Pa}(X_i),x_j)}$. We have:

$$\begin{aligned} &(\text{Pa}(X_i)\theta^1_{\boldsymbol{p}|\boldsymbol{p}j} + X_i\theta_{i|j}) - \text{Pa}(X_i)\theta_{\boldsymbol{p}|\boldsymbol{p}j} \\ &= \underbrace{(\text{Pa}(X_i)\theta^1_{\boldsymbol{p}|\boldsymbol{p}j} + (\text{Pa}(X_i)\theta^2_{\boldsymbol{p}|\boldsymbol{p}j} + E_{i|j}\theta_{i|j}))}_{(a)} - \underbrace{\text{Pa}(X_i)\theta_{\boldsymbol{p}|\boldsymbol{p}j}}_{(b)} \\ &= (\text{Pa}(X_i)\theta_{\boldsymbol{p}|\boldsymbol{p}j} + E_{i|j}\theta_{i|j}) - \text{Pa}(X_i)\theta_{\boldsymbol{p}|\boldsymbol{p}j} \\ &= E_{i|j}\theta_{i|j} = \phi_{i|j}, \end{aligned}$$

where we have decomposed $\theta_{\boldsymbol{p}|\boldsymbol{p}j}$ into $\theta^1_{\boldsymbol{p}|\boldsymbol{p}j}$ and $\theta^2_{\boldsymbol{p}|\boldsymbol{p}j}$ denoting the component of the total effect of $\text{Pa}(X_i)$ on Y in $\mathbb{G}_{\text{do}(\text{Pa}(X_i),x_j)}$ that does not and does pass through X_i, respectively. The second equality holds because $X_i\theta_{i|j}$ is equal to the total effect of $\text{Pa}(X_i)$ passing through X_i given by $\text{Pa}(X_i)\theta^2_{\boldsymbol{p}|\boldsymbol{p}j}$ plus the total effect of E_i given by $E_{i|j}\theta_{i|j}$. We encourage the reader to compare the third line of the above equation to the first line of Equation (5). The terms highlighted by the two underbraces prove the following theorem:

Theorem 3. *$\phi_{i|j}$ equals (a) the total effect of $\text{Pa}(X_i) \cup X_i$ on Y in the graph $\mathbb{G}_{\text{do}(X_i,\text{Pa}(X_i),x_j)}$ minus (b) the total effect of $\text{Pa}(X_i)$ on Y in the graph $\mathbb{G}_{\text{do}(\text{Pa}(X_i),x_j)}$ under the partially linear model.*

We compute the required total effects for any $\Delta_{i|j}$ from the coefficient matrix β and therefore recover all of the TREs Π.

D. Algorithm

Sections V-A through V-C lead to the Root and Treated Root causal Effects (R-TRE) algorithm, which we summarize in Algorithm 1. R-TRE first learns the DAG $\mathbb{G}$ and corresponding linear coefficient matrix β over $\text{Anc}(Y)$ in Line 1. We assume that we can recover $\mathbb{G}$ uniquely using any method of choice. In this paper, we use constraint-based search and orient any remaining undirected edges by experimentation or background knowledge [27].

R-TRE then intervenes on each X_j that can block the root causal effect of X_i on Y in Line 6; i.e., by intervening on those

Algorithm 1 Root and Treated Root causal Effects (R-TRE)

Input: $\boldsymbol{X}$
Output: ϕ, Π

1: Learn the causal graph $\mathbb{G}$ and coefficient matrix β
2: $\phi = 0; \Pi = 0$
3: **for each** $X_i \in \text{Anc}(Y) \setminus Y$ **do**
4: Compute ϕ_i via linear regression (or total effects) using Eq. (4)
5: **for each** $X_j \in \text{Dec}(X_i) \cap \text{Anc}(Y) \setminus Y$ **do**
6: Compute $\phi_{i|j}$ via total effects using Thm. 3
7: $\Pi_j \leftarrow \Pi_j + (\phi_{i|j} - \phi_i)$
8: **end for**
9: **end for**

vertices that are both a descendant of X_i and an ancestor of Y (excluding Y itself). This allows the algorithm to compute $\phi_{i|j}$ in Line 6 per Theorem 3. Finally, R-TRE adds in each $\Delta_{i|j}$ in Line 7 in order to recover the TREs Π.

E. Downstream Clustering

R-TRE outputs the TREs Π corresponding to the changes in the root causal effects after treatment. We can therefore discover theratypes from Π by performing hierarchical clustering on the feature space.

We seek clusters where patients respond similarly to treatment. We therefore perform agglomerative hierarchical clustering on Π using Ward's method [28]. Ward's method merges two clusters when the merge leads to a minimum increase in the (weighted) squared Euclidean distance between cluster means. As a result, Ward's method yields a dendogram where each cluster contains patients who respond similarly to the cluster mean.[1]

The dendogram importantly summarizes nested clusters so that users can identify large enough groups of patients who respond similarly to treatment. Each patient may respond to treatment differently, but categorizations help clinicians quickly comprehend patients by leveraging their past experiences with similar individuals. Recall that the partially linear model of Section IV-A allows discrete error terms that can induce clustering. Clear clusters may not exist in many cases, but we seek to identify them when they do. If a patient does not fall into a cluster, then we resort to a dimensional approach by directly utilizing the recovered TREs [29].

VI. Other Measures

We emphasize that the TREs recovered by the R-TRE algorithm differ from other measures introduced in the literature. We summarize the discussion in Table II in terms of four criteria – whether the method (1) involves causality, (2) attempts to detect root causes, (3) achieves precision or sample-specificity, or (4) accounts for targeted interventions on the endogenous variables.

Conditional and Marginal Shapley Values (CSV, MSV). [26], [30] These Shapley values quantify feature importance according to a trained model. The conditional and marginal Shapley values marginalize over the inputs of the model using conditional or marginal expectations, respectively. Authors have argued that marginal Shapley values better represent causal relations between *algorithm* input-output pairs [30]. Marginal Shapley values however do not represent the causality in *nature* required for TREs and disease subtyping.

Marginal Error term Shapley Values (MESV). [13]–[15], [25] These features correspond to marginal Shapley values on the error terms. Marginal error term Shapley values are equivalent to the root causal effects under a linear SEM provided that we can recover the error term values uniquely under invertibility. R-TRE recovers root causal effects even in the non-invertible scenario.

[1]We focus on interpretability with a dendogram, but users may employ alternative clustering methods depending on the needs of their particular application. The clusters must group patients who respond similarly to treatment.

	Causality	*Root Causes*	*Precision*	*Interventions*
MSV			✓	
CSV			✓	
MESV	✓	✓	✓	
ASV	✓		✓	
RCAO	✓	✓		
RCAM	✓	✓		
ICC	✓	✓	✓	
do-Reg	✓		✓	✓
do-SV	✓		✓	✓
Reg			✓	
Cor			✓	
TRE	✓	✓	✓	✓

TABLE II: Comparison against previously proposed measures.

Asymmetric Shapley Values (ASV). [23] Asymmetric Shapley values are conditional Shapley values that take into account natural causality by marginalizing over subsets of the ancestors of each variable. Asymmetric Shapley values therefore incorporate variable ordering. In contrast, R-TRE *always* conditions on *all* of the parents in order to explicitly recover root causal effects and TREs.

Root Causal Analysis of Outliers (RCAO) or Marginals (RCAM). [31], [32] These values quantify the contribution of the error terms on an outlier score or a marginal distribution. They therefore require an invertible SEM, forego sample-specificity and do not quantify root causal effects under interventions.

Intrinsic Causal Contribution (ICC). [33] ICC quantifies the reduction in uncertainty of a variable after knowing the value of an error term. This method therefore again assumes that we can recover the error term values uniquely from an invertible SEM.

do-Regression (do-Reg) and do-Shapley Values (do-SV). [24], [34] Do-regression computes $\mathbb{E}(Y|\text{do}(X_i))$ for each $X_i \in \boldsymbol{X} \setminus Y$ whereas do-Shapley values perform the do-operation across all subsets of $\boldsymbol{X} \setminus Y$. These algorithms perform interventions but do not specifically track for changes in root causal effects.

Standard Regression (Reg) and Correlation (Cor). We include standard multivariate linear regression and correlation (or univariate linear regression) as sanity checks. We weigh each feature by its regression coefficient.

We conclude that only TREs account for the change in root causal effects after performing targeted interventions, and R-TRE does not require an invertible SEM.

VII. Experiments

We now evaluate the accuracy of R-TRE and compare it against other algorithms recovering the measures of Section VI.

A. Data Generation

We first generated a linear SEM obeying Equation (2) with $p = 10$ variables. We created the coefficient matrix β by sampling from a Bernoulli$(2/(p-1))$ distribution in the upper

	$n = 1000$			$n = 3000$			$n = 9000$		
	RE	TRE	CTRE	RE	TRE	CTRE	RE	TRE	CTRE
MSV	0.1962	0.5246	1.3604	0.1907	0.5255	1.3617	0.1871	0.5252	1.3590
CSV	0.1630	0.4784	1.2285	0.1569	0.4796	1.2282	0.1534	0.4793	1.2256
MESV	**0.0878**	0.4798	1.2505	**0.0764**	0.4906	1.2763	**0.0570**	0.4999	1.2941
ASV	0.2336	0.5897	1.4588	0.2250	0.5890	1.4529	0.2214	0.5885	1.4486
RCAO	0.3482	0.3706	1.0883	0.3477	0.3701	1.0896	0.3279	0.3502	1.0340
RCAM	0.2484	0.2729	0.8189	0.2491	0.2734	0.8202	0.2492	0.2734	0.8202
ICC	0.3438	0.3637	1.0654	0.3335	0.3525	1.0416	0.3384	0.3578	1.0595
do-Reg	0.1254	0.5080	1.3254	0.1180	0.5170	1.3464	0.1074	0.5276	1.3662
do-SV	0.1046	0.4757	1.2587	0.0989	0.4870	1.2847	0.0873	0.4955	1.3007
Reg	0.1969	0.5250	1.3621	0.1912	0.5257	1.3625	0.1875	0.5254	1.3596
Cor	0.2129	0.5823	1.4483	0.2103	0.5830	1.4443	0.2086	0.5829	1.4405
R-TRE	**0.0934**	**0.0999**	**0.5701**	**0.0759**	**0.0784**	**0.5468**	**0.0568**	**0.0617**	**0.5381**

TABLE III: Mean RMSE results to the ground truth RE, TRE and CTRE values. Bolded values highlight the best performances. R-TRE achieves the lowest RMSE in all three cases across all sample sizes.

triangular portion of the matrix with an expected neighborhood size of 2. We then randomly permuted the variable ordering. We introduced weights β by uniformly sampling from $[-1, -0.25] \cup [0.25, 1]$. We chose the distributions of the error terms uniformly at random from the following set: a uniform distribution between -1 and 1, a t-distribution with three degrees of freedom, or a discrete uniform distribution with 2 or 3 values. We centered all error terms. We then binarized a random subset of the variables with at most one child to ensure a non-invertible SEM. We chose Y randomly from the set of random variables with at least one parent; Y need not be a terminal vertex. We repeated the above procedure 250 times for sample sizes 1000, 3000 and 9000. We therefore generated a total of $250 \times 3 = 750$ unique datasets.

Reproducibility. All code needed to reproduce the experimental results is available at https://github.com/ericstrobl/RTRE.

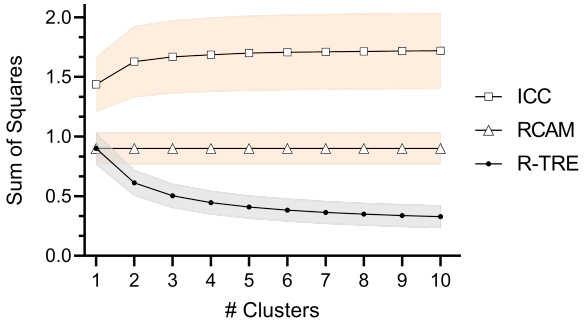

Fig. 1: Mean sum of squares across different cluster sizes for first, second and third place algorithms at $n = 9000$. Bands denote 95% confidence intervals. R-TRE continues to improve with increasing numbers of clusters, but the other two algorithms do not.

B. Comparators & Metric

We compare the output of R-TRE against algorithms recovering the eleven other measures listed in Table II. We learned the DAG for all algorithms using the PC algorithm equipped with the linear correlation test and an alpha threshold of 0.01 [27].

We evaluated the accuracy in recovering the root causal effects and the TREs using the root mean squared error (RMSE) to the ground truth:

$$\sqrt{\frac{1}{pn}\sum_{j=1}^{n}\sum_{i=1}^{p}\left(\widehat{\phi}_i^j - \phi_i^j\right)^2}, \qquad \sqrt{\frac{1}{pn}\sum_{j=1}^{n}\sum_{i=1}^{p}\left(\widehat{\Pi}_i^j - \Pi_i^j\right)^2},$$

where the superscripts index the n samples. We also evaluated the accuracy of the clustered TREs using the RMSE:

$$\sqrt{\frac{1}{10n}\sum_{k=1}^{10}\sum_{l=1}^{k}\sum_{j\in\mathcal{C}_l^k}\sum_{i=1}^{p}\left(\Pi_i^j - \frac{1}{|\mathcal{C}_l^k|}\sum_{j\in\mathcal{C}_l^k}\widehat{\Pi}_i^j\right)^2}.$$

The set $\mathcal{C}_l^k$ contains the sample indices of the l^{th} cluster among a total of k clusters. We vary k from 1 to 10. The above metric quantifies the distance from the true TREs to their estimated cluster means, i.e., the estimated treatment response by group. We collectively call these cluster means the *Clustered Treated Root causal Effects* (CTRE). We plot mean sum of squares (squared RMSE) for each k when varying the value of k in order to conform with tradition [28]. Lower values of the above three metrics denote better performance.

C. Results

We summarize the accuracy results in Table III. Bolded values denote the best performance according to a paired t-test significant at the Bonferonni corrected threshold of 0.05/12, since we compared a total of 12 algorithms. We place timing results in Table IV in the Appendix; R-TRE always completed within 10 milliseconds on average.

Root Causal Effects. Both R-TRE and MESV achieved the lowest RMSE in discovering the root causal effects (REs). MESV however requires access to the error terms, whereas R-TRE discovers the root causal effects using endogenous variables alone. The do-Shapley values came in third place and struggled to improve beyond the lowest tested sample size. We conclude that R-TRE accurately discovers sample-specific REs.

Treated Root Causal Effects. R-TRE outperformed all other algorithms by a large margin in estimating TREs; RCAM came

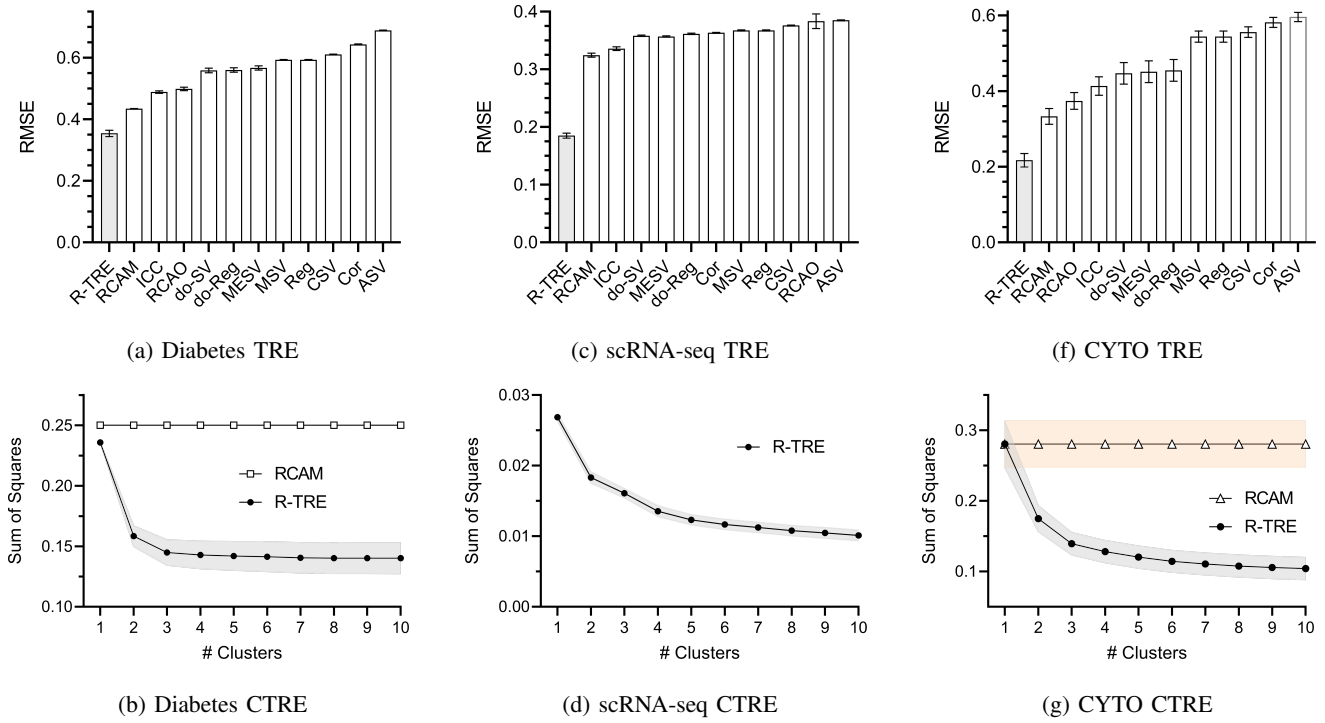

(a) Diabetes TRE (c) scRNA-seq TRE (f) CYTO TRE

(b) Diabetes CTRE (d) scRNA-seq CTRE (g) CYTO CTRE

Fig. 2: TRE and CTRE accuracy results for the real datasets. Error bars and bands again denote 95% confidence intervals.

in second place but with greater than 2.5 times the error. We conclude that R-TRE also accurately discovers sample-specific TREs.

Clustered Treated Root Causal Effects. Clustering results in loss of information due to the groupings. R-TRE however still outperformed all algorithms after clustering the estimated TREs from one to ten groups. We plot the accuracy results of the top three algorithms for up to 10 total clusters in Figure 1 for $n = 9000$; RCAM had a flat sum of squares line because its output is not sample-specific. Only the performance of R-TRE continued to improve with increasing numbers of clusters. We conclude that R-TRE accurately identifies samples with similar TREs regardless of total cluster number.

In summary, R-TRE outputs accurate REs, TREs and CTREs for target discovery. The algorithm outperforms all 11 other algorithms.

D. Applications

We demonstrate the generality of the approach by applying R-TRE and the other algorithms to a clinical dataset, a single-cell RNA sequencing (scRNA-seq) dataset and a flow cytometry dataset. We report the main results here but refer the reader to the Appendix for full tables of accuracy and timing results. We equipped the PC algorithm with a fast non-parametric conditional independence test for all real datasets [13], [35].

Type II Diabetes. We sought to identify TREs and theratypes in Type II diabetes using a real clinical dataset [36].[2] The dataset contains 7 variables related to the metabolic system in 768 Pima Indians; we excluded insulin due to a possible cycle involving insulin and glucose. Type II diabetes is well-studied, so we expect R-TRE to only identify one cluster of patients using clinical variables [37]. Note that multiple theratypes of type II diabetes likely exist, but they are not detectable when intervening on the routine clinical variables present in this dataset [38].

The dataset comes with a known ground-truth graph, which we used to fit the parameters of a linear SEM to obtain the ground truth [15]. We then ran all of the algorithms on 250 bootstrapped draws of the dataset. The algorithms only had access to the graph estimated from bootstrapped samples using PC. We did not intervene on age and pedigree for R-TRE, do-reg and do-SV, since we cannot intervene on these variables in practice.

We summarize results in Figures 2 (a) and 2 (b). R-TRE achieved the lowest mean RMSE to the ground truth TREs as compared to the 11 other algorithms (Figure 2 (a)). We plot the clustering results of the top two algorithms including R-TRE and RCAM in Figure 2 (b); the sum of squares for all other algorithms increased with increasing number of clusters implying worse performance. The clustering results of R-TRE in Figure 2 (b) show a sharp drop in the sum of squares after one cluster and a subsequent leveling off. R-TRE therefore only identified approximately one theratype in this dataset as expected. We conclude that R-TRE identified the correct number of clusters and estimated treatment effect most accurately in the Pima Indians dataset.

Single-Cell RNA Sequencing in Disease. We next sought to increase the difficulty by utilizing an scRNA-seq dataset

[2]https://www.kaggle.com/datasets/uciml/pima-indians-diabetes-database

of lung adenocarcinoma [39].[3] R-TRE is sample-specific in general, so we can use the algorithm to identify TREs of individual cells rather than just patients. The scRNA-seq dataset contains 17,502 single cells derived from cancerous and normal adjacent tissue in three individuals. We thus expect to detect *at least* three clusters of cells due to the heterogeneity of the cell population. We focused on variables involved in the mitogen-activated protein kinase (MAPK) pathway because of its importance in lung cancer pathogenesis. The variables include lung adenocarcinoma status as well as expression levels of GRB2, HRAS, ARAF, CCND1. We also included KRAS and TP53. We excluded EGFR since it had nearly all zero counts in the dataset. We extracted the ground truth causal graph from the KEGG pathway of non-small cell lung cancer (HSA05223) [40], [41].

We set lung adenocarconima status as the target. We report the results in the same format as with the previous example over 100 bootstrapped draws in Figures 2 (c) and 2 (d). R-TRE again estimated the TREs to the highest accuracy. Moreover, clustering results showed a gradual decline in the sum of squares rather than a leveling off. R-TRE identified at least 4 sub-populations of cells using the elbow method. We do not plot any other algorithms in Figure 2 (d) because they all performed much worse than R-TRE. We conclude that R-TRE achieved the highest accuracy and expected clustering results in this dataset.

Cell Signaling. The above two datasets use a diagnosis as a discrete terminal vertex. In this example, we demonstrate that R-TRE works well even if the target is continuous and non-terminal. We used the CYTO dataset which contains measurements of 11 phosphoproteins and phospholipids from 7466 primary human immune system cells across 9 experimental conditions [42], [43].[4] We standardized the data by mean and standard deviation in each experimental condition. The dataset again comes with a ground truth causal graph to fit a linear SEM. We chose the target uniformly at random for vertices that contain at least one parent. We do not expect to see a clear number of clusters in this case, since we vary the target. The inability to find well-defined clusters informs the user to examine the sample TRE values rather than adopt a categorical approach.

We summarize the results over 250 bootstrapped repetitions in Figures 2 (f) and 2 (g). R-TRE again achieved the lowest RMSE to the TREs by a large margin. Furthermore, clustering revealed a smooth decay in the sum of squares, suggesting that either many small or no meaningful groups exist in the data (Figure 2 (g)). We conclude that R-TRE works well across a variety of response variables, even if the cells fail to cluster into a few groups.

In summary, real data results indicate that R-TRE performs well across a variety of scenarios. The algorithm estimates the root causal effects and TREs accurately; it also identifies the theratypes we expect to see across three different dataset types.

[3]https://www.ncbi.nlm.nih.gov/geo/query/acc.cgi?acc=GSE123904

[4]https://arxiv.org/src/1805.03108v1/anc/data.txt

VIII. Conclusion

We summarized the causal effects involved in pathogenesis using root causal effects. We then quantified the response of the pathogenic mechanisms to treatment using TREs. We discovered theratypes by clustering samples with similar TREs. We finally automated these three ideas under a partially linear model with the R-TRE algorithm that simultaneously recovers root causal effects, TREs and CTREs. The algorithm importantly recovers the above quantities even in non-invertible SEMs, where we cannot recover the error term values exactly. Experimental results revealed substantially increased accuracy relative to existing algorithms. Future work will focus on extending R-TRE to the non-linear setting, accommodating confounding as well as incorporating high throughput experimentation in large scRNA-seq datasets.

References

[1] G. W. Imbens and D. B. Rubin, *Causal Inference in Statistics, Social, and Biomedical Sciences*. Cambridge University Press, 2015.

[2] J. Pearl, *Causality*. Cambridge: Cambridge University Press, 2009.

[3] A. Bhangu, K. Søreide, S. Di Saverio, J. H. Assarsson, and F. T. Drake, "Acute appendicitis: Modern understanding of pathogenesis, diagnosis, and management," *The Lancet*, vol. 386, no. 10000, pp. 1278–1287, 2015.

[4] K. B. Wray, *Resisting Scientific Realism*. Cambridge University Press, 2018.

[5] K. Jaspers, *General Psychopathology*. Johns Hopkins University Press, 1997, vol. 2.

[6] I. Kant, J. M. D. Meiklejohn, T. K. Abbott, and J. C. Meredith, *Critique of Pure Reason*. JM Dent London, 1934.

[7] I. Agache, C. A. Akdis, *et al.*, "Precision medicine and phenotypes, endotypes, genotypes, regiotypes, and theratypes of allergic diseases," *The Journal of Clinical Investigation*, vol. 129, no. 4, pp. 1493–1503, 2019.

[8] A. D. Sheftel, A. B. Mason, and P. Ponka, "The long history of iron in the universe and in health and disease," *Biochimica et Biophysica Acta (BBA)-General Subjects*, vol. 1820, no. 3, pp. 161–187, 2012.

[9] H. F. Bunn, "Vitamin b12 and pernicious anemia - the dawn of molecular medicine," *New England Journal of Medicine*, vol. 370, no. 8, pp. 773–776, 2014.

[10] K. Zhang, Z. Wang, J. Zhang, and B. Schölkopf, "On estimation of functional causal models: General results and application to the post-nonlinear causal model," *ACM Transactions on Intelligent Systems and Technology (TIST)*, vol. 7, no. 2, pp. 1–22, 2015.

[11] S. L. Lauritzen, A. P. Dawid, B. N. Larsen, and H.-G. Leimer, "Independence properties of directed markov fields," *Networks*, vol. 20, no. 5, pp. 491–505, 1990.

[12] S. Shimizu, P. O. Hoyer, A. Hyvärinen, A. Kerminen, and M. Jordan, "A linear non-gaussian acyclic model for causal discovery.," *Journal of Machine Learning Research*, vol. 7, no. 10, 2006.

[13] E. V. Strobl, "Counterfactual formulation of patient-specific root causes of disease," *arXiv preprint arXiv:2305.17574*, 2023.

[14] E. V. Strobl and T. A. Lasko, "Identifying patient-specific root causes of disease," in *Proceedings of the 13th ACM International Conference on Bioinformatics, Computational Biology and Health Informatics*, ser. BCB '22, Northbrook, Illinois: Association for Computing Machinery, 2022, ISBN: 9781450393867.

[15] E. V. Strobl and T. A. Lasko, "Sample-specific root causal inference with latent variables," *Causal Learning and Reasoning*, 2023.

[16] R. Macarron, M. N. Banks, D. Bojanic, *et al.*, "Impact of high-throughput screening in biomedical research," *Nature Reviews Drug Discovery*, vol. 10, no. 3, pp. 188–195, 2011.

[17] E. E. Schadt, S. H. Friend, and D. A. Shaywitz, "A network view of disease and compound screening," *Nature Reviews Drug Discovery*, vol. 8, no. 4, pp. 286–295, 2009.

[18] A.-L. Barabási, N. Gulbahce, and J. Loscalzo, "Network medicine: A network-based approach to human disease," *Nature Reviews Genetics*, vol. 12, no. 1, pp. 56–68, 2011.

[19] E. Guney, J. Menche, M. Vidal, and A.-L. Barábasi, "Network-based in silico drug efficacy screening," *Nature Communications*, vol. 7, no. 1, p. 10 331, 2016.

[20] M. H. Maathuis, M. Kalisch, and P. Bühlmann, "Estimating high-dimensional intervention effects from observational data," *The Annals of Statistics*, vol. 37, no. 6A, pp. 3133–3164, 2009. DOI: 10.1214/09-AOS685. [Online]. Available: https://doi.org/10.1214/09-AOS685.
[21] D. Malinsky and P. Spirtes, "Estimating causal effects with ancestral graph markov models," in *Conference on Probabilistic Graphical Models*, PMLR, 2016, pp. 299–309.
[22] T.-Z. Wang, T. Qin, and Z.-H. Zhou, "Sound and complete causal identification with latent variables given local background knowledge," *Advances in Neural Information Processing Systems*, vol. 35, pp. 10 325–10 338, 2022.
[23] C. Frye, C. Rowat, and I. Feige, "Asymmetric shapley values: Incorporating causal knowledge into model-agnostic explainability," *Advances in Neural Information Processing Systems*, vol. 33, pp. 1229–1239, 2020.
[24] Y. Jung, S. Kasiviswanathan, J. Tian, D. Janzing, P. Blöbaum, and E. Bareinboim, "On measuring causal contributions via do-interventions," in *International Conference on Machine Learning*, PMLR, 2022, pp. 10 476–10 501.
[25] E. V. Strobl and T. A. Lasko, "Identifying patient-specific root causes with the heteroscedastic noise model," *Journal of Computational Science*, vol. 72, 2023.
[26] S. M. Lundberg and S.-I. Lee, "A unified approach to interpreting model predictions," in *Proceedings of the 31st International Conference on Neural Information Processing Systems*, 2017, pp. 4768–4777.
[27] P. Spirtes, C. Glymour, and R. Scheines, *Causation, Prediction, and Search*, 2nd. MIT press, 2000.
[28] J. H. Ward Jr, "Hierarchical grouping to optimize an objective function," *Journal of the American Statistical Association*, vol. 58, no. 301, pp. 236–244, 1963.
[29] V. Peralta and M. J. Cuesta, "A dimensional and categorical architecture for the classification of psychotic disorders," *World Psychiatry*, vol. 6, no. 2, p. 100, 2007.
[30] D. Janzing, L. Minorics, and P. Blöbaum, "Feature relevance quantification in explainable ai: A causal problem," in *International Conference on Artificial Intelligence and Statistics*, PMLR, 2020, pp. 2907–2916.
[31] K. Budhathoki, D. Janzing, P. Bloebaum, and H. Ng, "Why did the distribution change?" In *International Conference on Artificial Intelligence and Statistics*, PMLR, 2021, pp. 1666–1674.
[32] K. Budhathoki, L. Minorics, P. Blöbaum, and D. Janzing, "Causal structure-based root cause analysis of outliers," in *International Conference on Machine Learning*, PMLR, 2022, pp. 2357–2369.
[33] D. Janzing, P. Blöbaum, L. Minorics, P. Faller, and A. Mastakouri, "Quantifying intrinsic causal contributions via structure preserving interventions," *arXiv e-prints*, 2020.
[34] T. Heskes, E. Sijben, I. G. Bucur, and T. Claassen, "Causal shapley values: Exploiting causal knowledge to explain individual predictions of complex models," *Advances in Neural Information Processing Systems*, vol. 33, pp. 4778–4789, 2020.
[35] E. V. Strobl, K. Zhang, and S. Visweswaran, "Approximate kernel-based conditional independence tests for fast non-parametric causal discovery," *Journal of Causal Inference*, vol. 7, no. 1, 2019.
[36] J. W. Smith, J. E. Everhart, W. Dickson, W. C. Knowler, and R. S. Johannes, "Using the adap learning algorithm to forecast the onset of diabetes mellitus," in *Proceedings of the Annual Symposium on Computer Application in Medical Care*, American Medical Informatics Association, 1988, p. 261.
[37] M. J. Davies, V. R. Aroda, B. S. Collins, *et al.*, "Management of hyperglycemia in type 2 diabetes, 2022. a consensus report by the american diabetes association (ada) and the european association for the study of diabetes (easd)," *Diabetes Care*, vol. 45, no. 11, pp. 2753–2786, 2022.
[38] S. Schrader, A. Perfilyev, E. Ahlqvist, *et al.*, "Novel subgroups of type 2 diabetes display different epigenetic patterns that associate with future diabetic complications," *Diabetes Care*, vol. 45, no. 7, pp. 1621–1630, 2022.
[39] A. M. Laughney, J. Hu, N. R. Campbell, *et al.*, "Regenerative lineages and immune-mediated pruning in lung cancer metastasis," *Nature Medicine*, vol. 26, no. 2, pp. 259–269, 2020.
[40] M. Kanehisa and S. Goto, "Kegg: Kyoto encyclopedia of genes and genomes," *Nucleic Acids Research*, vol. 28, no. 1, pp. 27–30, 2000.
[41] E. V. Strobl and T. A. Lasko, "Root causal inference from single cell rna sequencing with the negative binomial," in *Proceedings of the 14th ACM International Conference on Bioinformatics, Computational Biology and Health Informatics*, ser. BCB '23, Northbrook, Illinois: Association for Computing Machinery, 2023.
[42] K. Sachs, O. Perez, D. Pe'er, D. A. Lauffenburger, and G. P. Nolan, "Causal protein-signaling networks derived from multiparameter single-cell data," *Science*, vol. 308, no. 5721, pp. 523–529, 2005.
[43] J. Ramsey and B. Andrews, "Fask with interventional knowledge recovers edges from the sachs model," *arXiv preprint arXiv:1805.03108*, 2018.

APPENDIX

Proofs

Theorem 1. *The root causal effect of X_i on Y corresponds to the total effect of E_i on Y, or $E_i\theta_i$, under the partially linear model.*

Proof. We consider the Shapley value formulation introduced in [13]–[15], where:

$$S_i = \frac{1}{p} \sum_{\boldsymbol{W} \subseteq (\boldsymbol{E} \setminus E_i)} \frac{1}{\binom{p-1}{|\boldsymbol{W}|}} \left(\mathbb{E}(Y|\boldsymbol{W}, E_i) - \mathbb{E}(Y|\boldsymbol{W}) \right).$$

We have $Y = \boldsymbol{E}_{\mathrm{Anc}(Y)}\theta_{\mathrm{Anc}(Y)} + \boldsymbol{E}_{\boldsymbol{N}}\theta_{\boldsymbol{N}}$ under the partially linear model, where θ corresponds to the total effects of the error terms on Y, $\boldsymbol{N} = \boldsymbol{X} \setminus \mathrm{Anc}(Y)$ and $\theta_{\boldsymbol{N}} = 0$. We now invoke Corollary 1 of [26] to conclude that the root causal effect of X_i corresponds to $S_i = E_i\theta_i$. □

Lemma 1. *We have* $\mathbb{P}(Y|E_i, \mathrm{Pa}(X_i)) = \mathbb{P}(Y|X_i, \mathrm{Pa}(X_i))$.

Proof. We can write the following sequence of equalities:

$$\mathbb{P}(Y|E_i, \mathrm{Pa}(X_i)) = \mathbb{E}_{X_i|E_i,\mathrm{Pa}(X_i)}\mathbb{P}(Y|X_i, \mathrm{Pa}(X_i), E_i)$$
$$= \mathbb{P}(Y|X_i, \mathrm{Pa}(X_i), E_i) = \mathbb{P}(Y|X_i, \mathrm{Pa}(X_i)).$$

The second equality follows because X_i is a constant given E_i and $\mathrm{Pa}(X_i)$. We justify the last equality on a case-by-case basis:

(1) If X_i is an ancestor of Y, then the last equality holds because E_i and Y are conditionally independent given $X_i \cup \mathrm{Pa}(X_i)$ by the global Markov property.
(2) If X_i is not an ancestor of Y, then we have two subcases. If $Y \in \mathrm{Pa}(X_i)$, then E_i and Y are conditionally independent given $X_i \cup \mathrm{Pa}(X_i)$ because Y is a constant given $\mathrm{Pa}(X_i)$. If $Y \notin \mathrm{Pa}(X_i)$, then again E_i and Y are conditionally independent given $X_i \cup \mathrm{Pa}(X_i)$ by the global Markov property because E_i and Y are d-separated given $X_i \cup \mathrm{Pa}(X_i)$.

We have considered all cases, whence the conclusion follows. □

Other Experimental Results

	1000	3000	9000
MSV	0.1448	0.2679	0.6663
CSV	6.9661	11.624	31.391
MESV	0.0003	0.0013	0.0030
ASV	2.0513	2.8520	6.3738
RCAO	0.3281	0.5229	1.2834
RCAM	0.1785	0.3048	0.7790
ICC	2.1826	3.6168	7.9542
do-Reg	0.0007	0.0008	0.0022
do-SV	0.1315	0.1966	0.4026
Reg	0.0002	0.0006	0.0010
Cor	0.0004	0.0007	0.0031
R-TRE	0.0017	0.0021	0.0054

TABLE IV: Timing results for the synthetic data in seconds. Columns correspond to different sample sizes.

	Diabetes			scRNA-seq			CYTO		
	RE	TRE	CTRE	RE	TRE	CTRE	RE	TRE	CTRE
MSV	0.3431	0.5404	0.6694	**0.1260**	0.3674	0.2773	0.3242	0.5442	0.8805
CSV	0.4200	0.5617	0.6874	0.2647	0.3761	0.3012	0.3617	0.5560	0.8945
MESV	**0.3374**	0.4983	0.5940	0.1765	0.3569	0.2689	**0.2075**	0.4512	0.7362
ASV	0.5030	0.6283	0.8046	0.2702	0.3850	0.3111	0.4046	0.5960	1.008
RCAO	0.4509	0.4785	0.5909	0.3740	0.3835	0.3609	0.3413	0.3741	0.5258
RCAM	0.3774	0.3794	0.3907	0.3240	0.3246	0.2588	0.3312	0.3330	0.4393
ICC	0.5136	0.4836	0.5707	0.3114	0.3359	0.2549	0.4326	0.4135	0.6317
do-Reg	**0.3359**	0.5045	0.5973	0.1677	0.3615	0.2776	**0.2162**	0.4549	0.7472
do-SV	**0.3234**	0.4956	0.7251	0.1643	0.3582	0.2731	**0.2122**	0.4470	0.7251
Reg.	0.3430	0.5405	0.6699	0.1260	0.3674	0.2772	0.3241	0.5442	0.8806
Cor	0.3948	0.5809	0.7296	0.1366	0.3634	0.2712	0.3472	0.5818	0.9553
R-TRE	0.3565	**0.3642**	**0.3700**	0.1630	**0.1851**	**0.1181**	**0.2243**	**0.2175**	**0.3182**

TABLE V: Accuracy results for the real data.

	Diabetes	scRNA-seq	CYTO
MSV	0.0946	0.5997	0.6707
CSV	5.3320	29.653	45.676
MESV	0.0002	0.0043	0.0022
ASV	1.8635	7.2489	7.1502
RCAO	0.4762	5.6888	0.9319
RCAM	0.2501	2.6468	0.3252
ICC	2.5110	41.712	7.2634
do-Reg	0.0006	0.0048	0.0022
do-SV	0.0389	0.3003	0.4386
Reg	0.0002	0.0024	0.0013
Cor	0.0004	0.0038	0.0025
R-TRE	0.0018	0.0201	0.0038

TABLE VI: Timing results for the real data in seconds.